NuMA interaction with chromatin is vital for proper chromosome decondensation at the mitotic exit

Ashwathi Rajeevan, Riya Keshri, Sukriti Kapoor, and Sachin Kotak*
Department of Microbiology and Cell Biology, Indian Institute of Science, 560012 Bangalore, India

ABSTRACT **NuMA is an abundant long coiled-coil protein that plays a prominent role in spindle organization during mitosis. In interphase, NuMA is localized to the nucleus and hypothesized to control gene expression and chromatin organization. However, because of the prominent mitotic phenotype upon NuMA loss, its precise function in the interphase nucleus remains elusive. Here, we report that NuMA is associated with chromatin in interphase and prophase but released upon nuclear envelope breakdown (NEBD) by the action of Cdk1. We uncover that NuMA directly interacts with DNA via evolutionarily conserved sequences in its C-terminus. Notably, the expression of the DNA-binding–deficient mutant of NuMA affects chromatin decondensation at the mitotic exit, and nuclear shape in interphase. We show that the nuclear shape defects observed upon mutant NuMA expression are due to its potential to polymerize into higher-order fibrillar structures. Overall, this work establishes the spindle-independent function of NuMA in choreographing proper chromatin decompaction and nuclear shape by directly associating with the DNA.**

Monitoring Editor
Kerry Bloom
University of North Carolina, Chapel Hill

Received: Jun 25, 2020
Revised: Aug 13, 2020
Accepted: Aug 20, 2020

INTRODUCTION

In a eukaryotic cell, the nucleus is the largest organelle that harbors the genetic information and nonmembrane organelles that are essential for the existence of life. Recent work has shown that the proper structural organization and the mechanical properties of the nucleus are vital for gene regulation (Lammerding *et al.*, 2004; Nagano *et al.*, 2017; Nozaki *et al.*, 2017; Finn *et al.*, 2019; reviewed in Friedl *et al.*, 2011; Van Steensel and Belmont, 2017; Mirny *et al.*, 2019). Within the nucleus, chromatin is organized in a nonrandom manner into defined regions called chromosomal territories. These territories must be preserved during chromatin condensation and decondensation events at mitotic entry and exit for proper gene regulation (Gerlich *et al.*, 2003; reviewed in Wandke and Kutay, 2013; Antonin and Neumann, 2016; Shoaib *et al.*, 2020). In the past few years, several genes, for instance, PP1 phosphatase, PNUTS, and p97 AAA+ ATPase, have been linked with the proper chromatin decondensation during mitotic exit (Landsverk *et al.*, 2005; Ramadan *et al.*, 2007; Qian *et al.*, 2011; Vagnarelli *et al.*, 2011). However, our knowledge about the complete set of proteins and their mechanisms of action in chromosome decompaction at the mitotic exit remains incomplete (reviewed in Wandke and Kutay, 2013; Antonin and Neumann, 2016; Shoaib *et al.*, 2020).

The nuclear mitotic apparatus (NuMA) is a large protein (2115 amino acids) with two globular domains separated by a long coiled-coil domain (Yang *et al.*, 1992). It is estimated that approximately 10^6 molecules of NuMA are present in mammalian cells (Compton *et al.*, 1992; reviewed in Cleveland, 1995). NuMA is present in the nucleus during interphase. However, upon nuclear envelope breakdown (NEBD) in mitosis, it localizes at the spindle poles and the cell cortex, where it is required for the proper assembly and maintenance of the mitotic spindle as well as spindle orientation and elongation (Lydersen and Pettijohn, 1980; Yang and Snyder, 1992; Compton and Cleveland, 1993; Merdes *et al.*, 1996; Merdes *et al.*, 2000; Woodard *et al.*, 2010; Kiyomitsu and Cheeseman, 2012; Kotak *et al.*, 2012, 2014; Seldin *et al.*, 2013; Zheng *et al.*, 2014; Hueschen *et al.*, 2019). Because NuMA is present as an abundant protein in interphase nuclei, several research groups have studied NuMA's function in the nucleus (Merdes and Cleveland, 1998; Harborth *et al.*, 2000; Abad *et al.*, 2007; Chandramouly *et al.*, 2007;

This article was published online ahead of print in MBoC in Press (http://www.molbiolcell.org/cgi/doi/10.1091/mbc.E20-06-0415) on August 26, 2020.

*Address correspondence to: Sachin Kotak (sachinkotak@iisc.ac.in).

Abbreviations used: Cdk1, cyclin-dependent kinase 1; FRAP, fluorescence recovery after photobleaching; NEBD, nuclear envelope breakdown; NER, nuclear envelope reformation; NLS, nuclear localization signal; NuMA, nuclear mitotic apparatus protein; Plk1, polo-like kinase 1; RCC1, regulator of chromosome condensation 1.

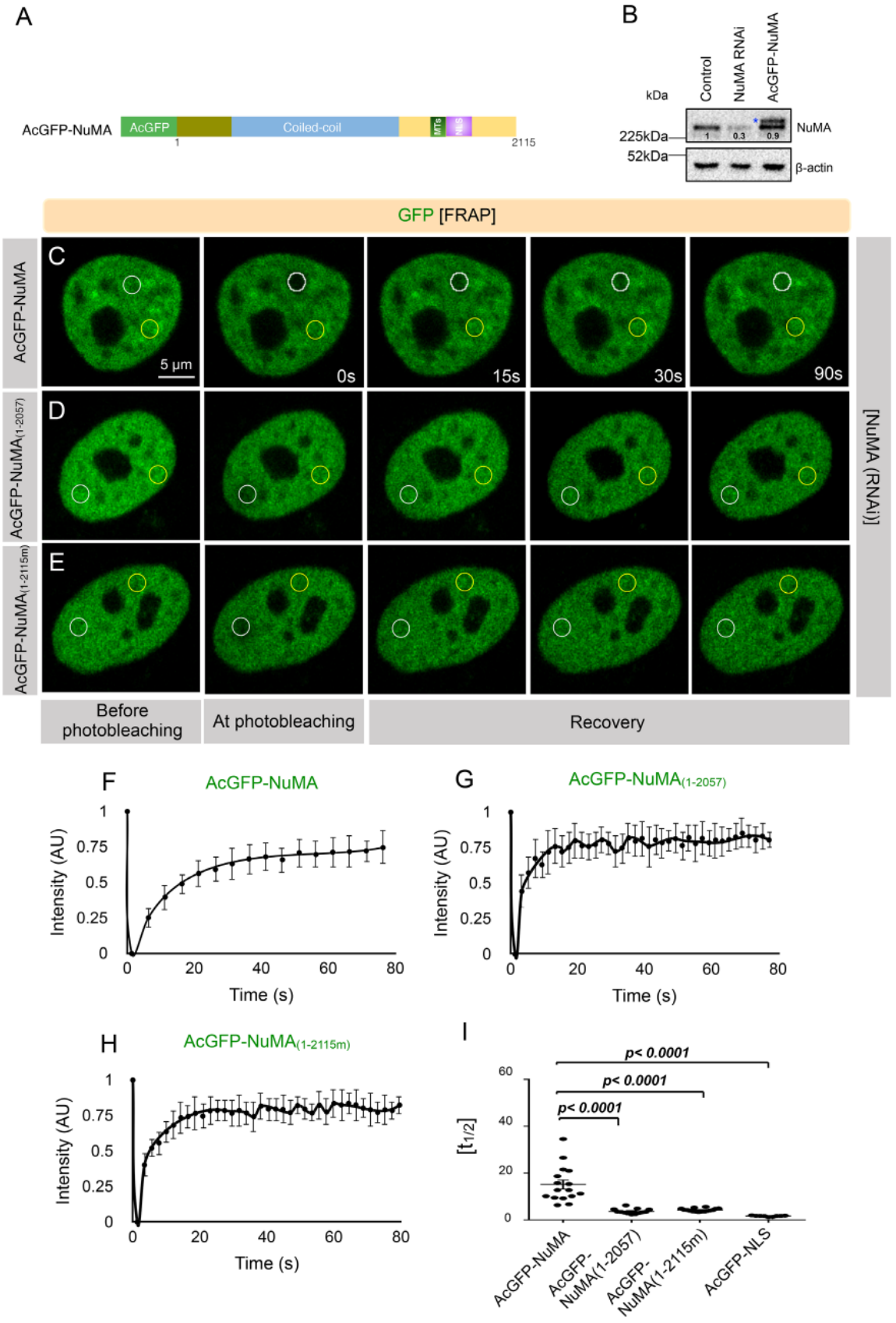

FIGURE 1: NuMA is transiently associated with chromatin in the interphase nucleus. (A) Domain organization of NuMA with mono-FLAG (FL) and AcGFP-tag at the N-terminus (referred to as AcGFP-NuMA). The coiled-coil domain, the region mediating interaction with microtubules (MTs), and the nuclear localization signal (NLS) are shown. (B) Immunoblot analysis of protein extracts prepared from the mitotically synchronized HeLa Kyoto cells, which are transfected with scrambled siRNAs (Control), siRNAs against NuMA 3′-UTR for 72 h, or left untreated and stably expressing AcGFP-NuMA. Extracts were probed with antibodies against NuMA and β-actin. Transgenic AcGFP-NuMA

Ohata *et al.*, 2013; Vidi *et al.*, 2014; Jayaraman *et al.*, 2017; Salvador Moreno *et al.*, 2019; reviewed in Radulescu and Cleveland, 2010). Within the nucleus, NuMA was proposed to be a part of a nuclear matrix, that is, an insoluble 3D network resistant to nucleases and high salt (Price and Pettijohn, 1986; Zeng *et al.*, 1994; Merdes and Cleveland, 1998). This finding was further supported by structural analysis showing that NuMA can form multiarm oligomers with its coiled-coil and C-terminus domain, and overexpression of NuMA creates a quasihexagonal organization that can fill the nuclei (Harborth *et al.*, 1999). Additionally, NuMA has been shown to co-localize with several nuclear proteins, including high mobility group proteins (HMG I/Y), transcription factor GAS41 and p53, suggesting its function in gene regulation (Harborth *et al.*, 2000; Tabellini *et al.*, 2001; Endo *et al.*, 2013; Ohata *et al.*, 2013). Recent reports have also indicated that NuMA is involved in DNA repair by regulating the accumulation of 53BP1 and ISW1 ATPase SNF2h on the double-strand breaks (Vidi *et al.*, 2014; Salvador Moreno *et al.*, 2019). These findings suggest that NuMA may directly or indirectly associate with the chromatin in the nucleus. Indeed, NuMA was shown to interact with chromatin biochemically (Abad *et al.*, 2007). However, the underlying mechanisms and the biological significance of this interaction have remained elusive. Microinjection of anti-NuMA antibodies against the C-terminus of NuMA or the expression of the truncated form of NuMA caused nuclear shape and organization defects (Kallajoki *et al.*, 1991; Compton and Cleveland, 1993; Kallajoki *et al.*, 1993; Gueth-Hallonet *et al.*, 1998). However, whether these defects were due to compromised mitosis upon NuMA inactivation remained unclear (reviewed in Radulescu and Cleveland, 2010).

In this study, we reveal that NuMA is associated with chromatin in interphase and prophase. Moreover, we show that in prophase, Cdk1/cyclinB1 (referred to as Cdk1) -mediated phosphorylation releases NuMA from chromatin. Importantly, we identify evolutionarily conserved sequences rich in arginine and lysine at the C-terminus of NuMA that enable NuMA to interact with DNA directly. Moreover, the expression of a mutant NuMA lacking the DNA-binding potential impacts chromatin decondensation during nuclear envelope reformation (NER). Additionally, this mutated NuMA undergoes higher-order assemblies and forms a puncta and solid fibrillar structure that perturbs nuclear shape. Overall, this study establishes a novel role of NuMA in chromosomes decompaction and nuclear architecture, and this function of NuMA appears to be independent of its role in spindle organization.

RESULTS

NuMA interacts with chromatin in interphase nuclei

To investigate the mobility of NuMA in the interphase nucleus, we sought to conduct a fluorescence recovery after photobleaching (FRAP) analysis in the HeLa cell line that stably expresses AcGFP (Aequorea coerulescens GFP), and a mono-FLAG tagged NuMA (AcGFP-NuMA; Figure 1A; Keshri *et al.*, 2020). This engineered line expresses AcGFP-NuMA, which is comparable to that of the endogenous protein (Figure 1B). siRNA-mediated depletion of endogenous NuMA led to chromosome instability and the appearance of chromosome bridges in a significant number of cells during mitosis, and these phenotypes were fully rescued in cells expressing AcGFP-NuMA, indicating that this cell line is fully functional (Supplemental Figure S1, A–C, F, and G). FRAP analysis in this line revealed that the half-time for the recovery ($t_{1/2}$) of AcGFP-NuMA is ~13 s (Figure 1, C, F, and I). The $t_{1/2}$ values for AcGFP-NuMA are in stark contrast to freely diffusible AcGFP-NLS (nuclear localization signal), where the $t_{1/2}$ value was estimated to be ~1.5 s (Figure 1I and Supplemental Figure S1, H and I). The $t_{1/2}$ value of AcGFP-NuMA is similar to that of various transcription factors that are transiently associated with the chromatin in interphase (reviewed in Houtsmuller, 2005; Hager *et al.*, 2009). These data suggest that NuMA could be associated with the chromatin inside the interphase nucleus in a living cell.

To corroborate this finding with biochemical means, we isolated chromatin and the nuclear matrix (a nonchromatin, ribonucleoproteinaceous framework that is resistant to high salt; see *Materials and Methods* for the detailed protocol) from interphase nuclei and analyzed the association of NuMA in these fractions. As reported previously, we noted that NuMA is associated with the nuclear matrix (Supplemental Figure S1J; Das *et al.*, 1993; Zeng *et al.*, 1994; Abad *et al.*, 2007). Interestingly, a significant amount of NuMA was also associated with the chromatin fraction in HeLa cells (Supplemental Figure S1J). A similar observation was made earlier in mammary epithelium cells (Abad *et al.*, 2007). Altogether these data suggest that NuMA is not freely diffusing inside the interphase nucleus, and this could be because of its interaction with the chromatin.

Cdk1-mediated phosphorylation release NuMA from chromatin at mitotic entry

During interphase, NuMA is present in the nucleus (Lydersen and Pettijohn, 1980; Kallajoki *et al.*, 1992; Tang *et al.*, 1993). However, in mitosis upon NEBD, NuMA localizes to the spindle poles and the cell cortex (Lydersen and Pettijohn, 1980; Compton *et al.*, 1992; Compton and Cleveland, 1993; Merdes *et al.*, 1996; Du and Macara, 2004; Woodard *et al.*, 2010; Kiyomitsu and Cheeseman, 2012; Kotak *et al.*, 2012). Data obtained from FRAP and biochemical analysis indicated that NuMA might be associated with chromatin in interphase. Thus, we wondered whether we can visualize this interaction in a living cell. Chromosomes are present in the least condensed state during interphase and appear as distinct bodies in prophase (reviewed in Batty and Gerlich, 2019). Therefore, we sought to examine the localization of NuMA in a synchronized

protein is shown by a blue asterisk that is migrating above the endogenous protein. The values below the NuMA immunoblot represent the band intensity with respect to the intensity value from the control sample, which was kept as 1. The molecular mass is indicated in kilodaltons (kDa). (C–I) FRAP analysis of HeLa Kyoto cells that are stably expressing AcGFP-NuMA (C, F), transiently transfected with AcGFP-NuMA$_{(1–2057)}$ (D, G) or AcGFP-NuMA$_{(1–2115m)}$ (E, H) and are depleted for endogenous NuMA. The GFP signal is shown in green, and the time is indicated in seconds (s). The unbleached and bleached regions of the cell are shown by yellow and white circles, respectively. The GFP recovery profile of the bleached area corrected for photobleaching is plotted for 80 s for all three conditions. Note the half-time of recovery ($t_{1/2}$) of cells expressing AcGFP-NuMA is ~13 s, which is remarkably slow in comparison with AcGFP-tagged NLS (nuclear localization signal) -expressing cells ($t_{1/2}$ = ~1.5 s) (I). Analogous $t_{1/2}$ value (~12.2 s) was obtained in cells which are transiently transfected with AcGFP-NuMA (unpublished data). Also, note that rapid recovery profile in cells expressing AcGFP-NuMA$_{(1–2057)}$ ($t_{1/2}$ = ~3.6 s) or AcGFP-NuMA$_{(1–2115m)}$ ($t_{1/2}$ = ~4.2 s) in comparison to that of AcGFP-NuMA (I). Statistical significance is calculated by two-tailed Student's *t* test ($n > 10$ for all; error bars: SD for F–H and SEM for I).

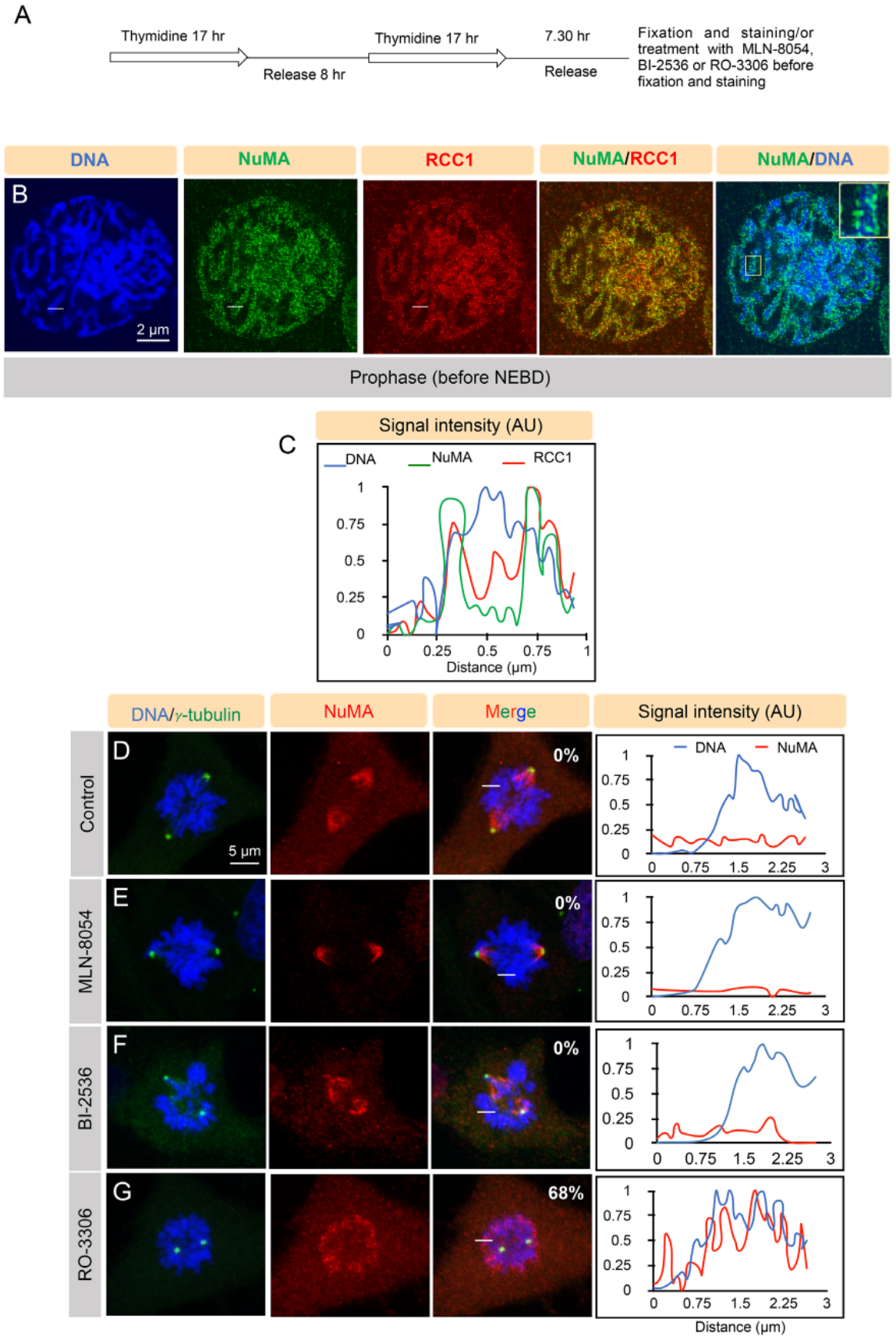

FIGURE 2: Cdk1 activity is critical for releasing NuMA from chromatin upon mitotic entry. (A) hTERT-RPE1 cell synchronization scheme for enriching cells in the prophase following double-thymidine release. Cells were fixed after 7.30 h of double-thymidine release for obtaining a maximum number of cells in prophase. Cells were treated with DMSO (Control), Aurora A inhibitor MLN-8054 (250 nM for 1 h), Plk1 inhibitor BI-2536 (300 nM for 30 min), or Cdk1 inhibitor RO-3306 (20 μM for 10 min) before fixation. (B) Higher-resolution images of prophase synchronized

prophase population of nontransformed hTERT-RPE1 cells (Figure 2A). Importantly, we found that NuMA significantly enriches onto chromosomes in prophase, and colocalizes with another chromatin-associated protein RanGEF RCC1 (Supplemental Figure S2A). Similar results were obtained in HeLa cells (unpublished data). To scrutinize this observation further, we analyzed the localization of DNA, NuMA, and RCC1 at a higher resolution in prophase cells. Data obtained from such analysis revealed that NuMA enriches at the periphery of condensed chromatin in prophase cells and colocalizes with RCC1 (Figure 2, B and C). Importantly, we also found that the GFP-tagged C-terminus of NuMA (GFP-NuMA$_{(1411–2115)}$), but not the N-terminus (GFP-NuMA$_{(1–705)}$) or the middle portion containing the large coiled-coil domain (GFP-NuMA$_{(706–1699)}$) localizes to chromatin in prophase (Supplemental Figure S2D; unpublished data). These results indicate that NuMA interacts with chromatin through its C-terminus.

Using temperature-sensitive hamster cell line tsBN2 that is affected for RCC1 at the restrictive temperature (Nishimoto *et al*., 1978; Nishitani *et al*., 1991), it was hypothesized that NuMA might interact with RCC1 or RCC1-dependent protein (Compton and Cleveland, 1993). Because NuMA showed a significant colocalization with RCC1, we investigated whether NuMA or RCC1 are interdependent for their chromatin localization in prophase nuclei. Interestingly, RNAi-mediated depletion of RCC1 or NuMA did not perturb NuMA or RCC1 localization onto chromatin, indicating that NuMA localization on chromatin is independent of RanGEF RCC1 (compare Supplemental Figure S2, B and C with A).

At mitotic entry, spatiotemporal localization of several proteins is regulated by the action of many different mitotic kinases. These kinases remodel the mitotic proteome, and thus assist in mitotic entry (reviewed in Lindqvist *et al*., 2009; Cuijpers and Vertegaal, 2018). Therefore, we wondered whether a kinase is involved in mediating NuMA release from the chromatin upon NEBD. To this end, we acutely inactivated the mitotic kinases such as Aurora A, Plk1, and Cdk1 in a synchronized G2/prophase population using MLN-8054, BI-2536, and RO-3306, respectively, and analyzed NuMA localization after NEBD in prometaphase (Figure 2A; Vassilev *et al*., 2006; Hoar *et al*., 2007; Steegmaier *et al*., 2007). Inactivation of Cdk1, but not Aurora A or Plk1, resulted in the retention of NuMA on the chromosomes during prometaphase (Figure 2, D–G). The inability of Aurora A or Plk1 inhibition to restore NuMA localization cannot be due to partial inactivation of these kinases because 1) we noted a robust impact of Aurora A inactivation on the spindle pole pool of NuMA, and Plk1 inactivation on the central spindle localization of a RhoGEF ECT2, as reported previously (Supplemental Figure S3, A–F; Petronczki *et al*., 2007; Kotak *et al*., 2016); and 2) identical results were obtained with a fivefold higher dose of these inhibitors (Supplemental Figure S3, G–J).

Next, to test whether direct phosphorylation of NuMA by Cdk1 would release NuMA from chromatin, we individually mutated nine threonine or serine residues that were identified as potential Cdk1 phosphorylation sites in a recent phosphoproteomics data set to alanine (Supplemental Figure S3K; Dephoure *et al*., 2008; Rogers *et al*., 2015; Petrone *et al*., 2016). However, we failed to identify a single Cdk1 site that uncouples NuMA from chromatin (please see *Discussion*). Although the exact mechanism by which Cdk1 phosphorylation uncouples NuMA from the chromatin upon mitotic entry will be of interest for future work, our current data supports the notion that Cdk1 activity is vital for releasing NuMA from the chromatin upon mitotic entry.

NuMA directly interacts with the DNA through its C-terminus

GFP-tagged C-terminus fragment of NuMA (GFP-NuMA$_{(1411–2115)}$) localizes onto chromatin in prophase, but not in prometaphase and metaphase (Figure 3, A and B, Supplemental Figure S4, A and B, and Supplemental Movie S1; Kotak *et al*., 2013; Sana *et al*., 2018). Therefore, we decided to identify a minimum signature sequence of NuMA in its C-terminus that may allow it to associate with the chromatin independent of the mitotic stages. To achieve this, we generated several GFP-fusion C-terminus fragments of NuMA and analyzed their localization at various stages of mitosis (Figure 3, A and C–F, and Supplemental Figure S4, C–J). Interestingly, in comparison to NuMA$_{(1411–2115)}$, the expression of NuMA$_{(1760–2115)}$ and NuMA$_{(1991–2115)}$ showed significant enrichment onto chromatin even in prometaphase and metaphase (compare Figure 3, D and E with 3B; Supplemental Figure S4, E–H). This analysis further demonstrated that the sequence comprising of the last 58 amino acids (2058–2115) is sufficient for its interaction with the chromatin in prophase, prometaphase, and in metaphase (Figure 3, F and G, Supplemental Figure S4, I and J, and Supplemental Movie S2). Next, we sought to determine whether sequences 2058–2115 are necessary for NuMA localization at the chromatin in prophase. Importantly, the one-third C-terminus fragment of NuMA (NuMA$_{(1411–2115)}$) that distinctly localizes on the condensed chromatin in prophase is incapable of doing so if the 2058–2115 region is missing (compare Figure 3I with H; Supplemental Movie S3). Similarly, the robust localization of NuMA$_{(1760–2115)}$ on metaphase chromosomes is lost when these last 58 amino acids are omitted from the sequence (Supplemental Figure S4, K–M). Altogether, these data strongly suggest that NuMA interaction with chromatin in prophase is via the last 58 amino acids in its C-terminus.

Sequence 2058–2115 is evolutionarily conserved, and rich in the positively charged arginine and lysine residues (Figure 3J). Therefore, one possibility could be that these amino acids directly interact with the acidic DNA sequences, enabling NuMA–DNA

hTERT-RPE1 cells immunostained for NuMA (green) and RanGEF RCC1 (red). DNA is visualized in blue (see *Materials and Methods*). Inset on the upper right on the merge between NuMA and DNA shows that NuMA enriches at the periphery of condensed chromatin in prophase cells. (C) Line-scan plot of DNA (in blue), NuMA (in green), and RCC1 (in red) was created using an area shown as a white line in panel B. Similarly for the other figures, a white line on the images represents the area that was utilized to make a line-scan plot. (D–G) hTERT-RPE1 cells synchronized in prophase, as indicated in panel A, are treated either with DMSO control (D), MLN-8054 (E), BI-2536 (F), or RO-3306 (G). After fixation, these cells are stained for NuMA (red) and γ-tubulin (green). The percentage of cells showing chromosomal retention of NuMA signal in cells treated with the various inhibitors is indicated on the corresponding images in the merge panel. Line-scan plots on the right represent the DNA and NuMA intensity for an area that is represented by the white line under various conditions. Note the retention of NuMA on chromatin in prometaphase cells that were treated with Cdk1 inhibitor RO-3306 compared with the control cells. Also, check Supplemental Figure S3 for control experiments ($n > 20$ cells in each condition and experiments were repeated four times).

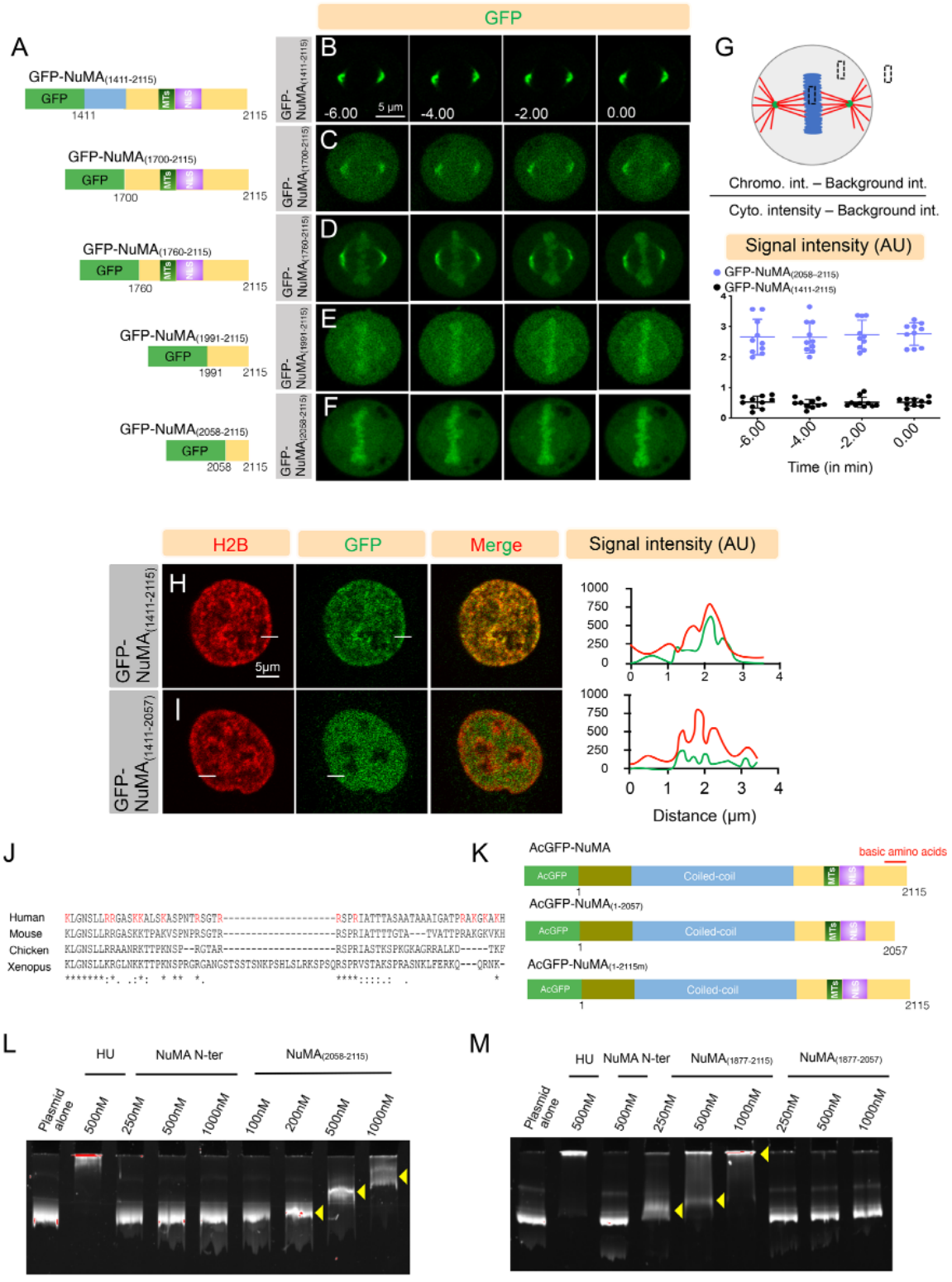

FIGURE 3: NuMA interacts with the DNA with the evolutionarily conserved region present in its C-terminus. (A) Schematic representation of GFP-tagged NuMA constructs used for the experiments that are shown on the right; the regions mediating interaction with microtubules (MTs), and the nuclear localization signal (NLS) are represented. (B–F) Images from the 4D time-lapse confocal microscopy of HeLa cells stably expressing mCherry-H2B and transiently transfected with GFP-NuMA$_{(1411–2115)}$ (B), GFP-NuMA$_{(1700–2115)}$ (C), GFP-NuMA$_{(1760–2115)}$ (D), GFP-NuMA$_{(1991–2115)}$ (E), or GFP-NuMA$_{(2058–2115)}$ (F). The GFP signal is shown in green. Time is indicated in minutes with $t = 0$ corresponding to the last frame of metaphase before the onset of chromosome segregation. Note the enrichment of GFP signal on the metaphase chromosome for cells expressing GFP-NuMA$_{(1760–2115)}$, GFP-NuMA$_{(1991–2115)}$, and GFP-NuMA$_{(2058–2115)}$. (G) Chromosomal intensity quantification scheme of a metaphase cell; black boxes indicate the area used for the quantification of the signal intensity. The ratio of the chromosomal to cytoplasmic GFP-signal intensity is plotted over time for GFP-NuMA$_{(1411–2115)}$ and GFP-NuMA$_{(2058–2115)}$. $p < 0.0001$ between GFP-NuMA$_{(1411–2115)}$ and

interaction. To test this, we generated Hexa-histidine-tagged 58 aa recombinant protein (6HIS-NuMA$_{(2058–2115)}$) in *Escherichia coli* and analyzed its potential to interact with DNA in a gel mobility shift assay. We uncovered that recombinant protein 6HIS-NuMA$_{(2058–2115)}$, but not a recombinant protein for NuMA N-terminus, interacts with plasmid DNA in vitro (Figure 3L). Importantly, the interaction of 6HIS-NuMA$_{(1877–2115)}$ with plasmid DNA is lost when the last 58 amino acids are deleted from this fragment (6HIS-NuMA$_{(1877–2057)}$; Figure 3M).

Next, to scrutinize the role of NuMA's DNA-binding ability in the context of the full-length protein, we conducted a FRAP analysis with AcGFP-tagged full-length NuMA lacking the last 58 amino acids (AcGFP-NuMA$_{(1–2057)}$; Figure 3K). Remarkably, the FRAP analysis revealed that AcGFP-NuMA$_{(1–2057)}$ shows greater mobility ($t_{1/2}$ = ~3.6 s) in the interphase nucleus when compared with AcGFP-NuMA ($t_{1/2}$ = ~13 s; Figure 1, D, G, and I). This observation suggests that the last 58 amino acids are crucial for NuMA's interaction with the chromatin, and most likely, this interaction restricts NuMA mobility inside the interphase nucleus. Furthermore, a FRAP analysis with a mutant NuMA where all 14 basic amino acid residues between 2058 and 2115 were mutated to alanine (AcGFP-NuMA$_{(1–2115m)}$; Figure 3K) revealed similar mobility profiles as AcGFP-NuMA$_{(1–2057)}$ (Figure 1, E, H, and I). This observation indicates that indeed, the presence of positively charged amino acids in the C-terminus of NuMA enables NuMA–DNA interaction in interphase nuclei.

NuMA–DNA interaction is crucial for proper chromosome decondensation at the mitotic exit

Upon NER, NuMA localizes back to the nucleus because of the presence of NLS in its C-terminus (reviewed in Cleveland, 1995; Radulescu and Cleveland, 2010). Because NuMA$_{(1–2057)}$ is incapable of interacting with DNA, and thus chromatin, we sought to analyze the relevance of NuMA–chromatin interaction upon NER. Importantly, in comparison to cells that express the full-length protein, expression of either AcGFP-NuMA$_{(1–2057)}$ or AcGFP-NuMA$_{(1–2115m)}$ in cells depleted for endogenous NuMA led to failure in chromosome decondensation at mitotic exit (Figure 4, A–C, and Supplemental Movies S4–S6). In these mutants, chromosomes remained significantly compact as evaluated by measuring the volume of the segregated chromosomal mass (Figure 4D). The impact of mutant NuMA expression on chromosome decondensation is not due to the failure or a delay of mutant NuMA protein to localize to the nucleus (unpublished data). Next, we attempted to assess the significance of NuMA's DNA-binding ability for chromosome decompaction and its impact on the nuclear shape in the early G1 phase of the cell cycle. For this purpose, we imaged HeLa cells after anaphase onset that were stably expressing nuclear envelope marker mCherry-LaminB1 and are transiently transfected either with the AcGFP-NuMA or AcGFP-NuMA$_{(1–2057)}$ in endogenous NuMA-depleted condition (Figure 4, E and F). Interestingly, the nuclear volume of cells expressing the mutant form of NuMA that is deficient in interacting with the DNA was significantly reduced in comparison with the cells that express the wild-type protein (Figure 4, E–H).

The effect of the expression of AcGFP-NuMA$_{(1–2057)}$ on chromatin decondensation at the mitotic exit or early G1 prompted us to analyze the shape of the interphase nuclei. Notably, we uncovered cells that express AcGFP-NuMA$_{(1–2057)}$ in NuMA (RNAi) background had an irregular nuclear shape in comparison to ones expressing full-length protein (Figure 4, I–L). The impact of NuMA$_{(1–2057)}$ expression on the nuclear shape cannot be due to its function in spindle assembly or maintenance as 1) NuMA$_{(1–2057)}$ localizes analogous to the full-length protein on the spindle pole, and more importantly 2) expression of this construct fully rescues the mitotic abnormalities seen upon endogenous NuMA depletion (Supplemental Figure S1, A–G). Interestingly, a significant number of cells expressing AcGFP-NuMA$_{(1–2057)}$ that showed an irregular nuclear shape were also characterized by the presence of puncta or a fibrillar structure in the nucleus (Figure 4, J and K). These structures were never seen in cells expressing full-length protein (Figure 4I). Also, the presence of these structures upon AcGFP-NuMA$_{(1–2057)}$ expression is not because of overexpression, as comparable expression of AcGFP-NuMA in cells did not lead to the appearance of such structures in the nucleus (Supplemental Figure S5, A–E). Overall, these data suggest that NuMA–DNA interaction is vital for DNA decondensation during mitotic exit, and also for the proper nuclear shape in interphase.

DNA-binding ability of NuMA is essential to prevent higher-order assemblies in interphase nuclei

A significant number of nuclei expressing the DNA-binding defective mutant of NuMA showed higher-order assemblies into puncta and fibrillar networks. To characterize the origin of these structure in cells expressing the DNA-binding–deficient mutant of NuMA, we conducted a live recording of HeLa cells that were stably expressing mCherry-H2B and were transiently transfected either with AcGFP-NuMA or AcGFP-NuMA$_{(1–2057)}$. In such analysis, we

GFP-NuMA$_{(2058–2115)}$ for all the time points studied. Statistical significance is calculated by two-tailed Student's *t* test (n = 10 cells for all cases; error bars: SD). (H, I) Images from the 4D-time-lapse confocal microscopy of HeLa cells in prophase before nuclear envelope breakdown (NEBD) that are stably expressing mCherry-H2B and transiently transfected with GFP-NuMA$_{(1411–2115)}$ (H) or GFP-NuMA$_{(1411–2057)}$ (I). Note that the GFP signal is homogeneously distributed in the nucleus in GFP-NuMA$_{(1411–2057)}$ expressing cells in comparison to the cells expressing GFP-NuMA$_{(1411–2115)}$ where the signal is localized to chromatin. Line-scan plot is shown on the right. (J) Sequence alignments of NuMA DNA-binding region (2058–2115) with NuMA orthologues (*Homo sapiens* NM_006185.2, *Mus musculus* NP_598708.3, *Gallus gallus* NP_001177854.1, *Xenopus laevis* NP_001081559.1). The basic amino acids (arginine and lysine residues) are highlighted in red. Note that the majority of basic amino acids are conserved across these species. (K) Schematic representation of AcGFP-tagged full-length NuMA (AcGFP-NuMA) or NuMA that is either deleted (AcGFP-NuMA$_{(1–2057)}$) or mutated (AcGFP-NuMA$_{(1–2115m)}$) for the last 58 aa. The coiled-coil domain, the region mediating interaction with microtubules (MTs), and the nuclear localization signal (NLS) are shown. (L, M) Gel mobility shift assay of pUC19 plasmid (400 ng) that is incubated with the indicated concentration of *E. coli*–generated recombinant proteins against bacterial histone-like protein HU, hexahistidine-NuMA N-ter (indicated as NuMA N-ter), and hexahistidine-NuMA$_{(2058–2115)}$ (indicated as NuMA$_{(2058–2115)}$) (L). Or with HU, NuMA N-ter, hexahistidine-NuMA$_{(1877–2115)}$ (indicated as NuMA$_{(1877–2115)}$), and hexahistidine-NuMA$_{(1877–2057)}$ (indicated as NuMA$_{(1877–2057)}$) (M). Yellow arrowheads indicate the retardation of pUC19 plasmid DNA upon the increasing concentration of NuMA$_{(2058–2115)}$ and NuMA$_{(1877–2115)}$, but not with NuMA$_{(1877–2057)}$ missing the last 58 aa.

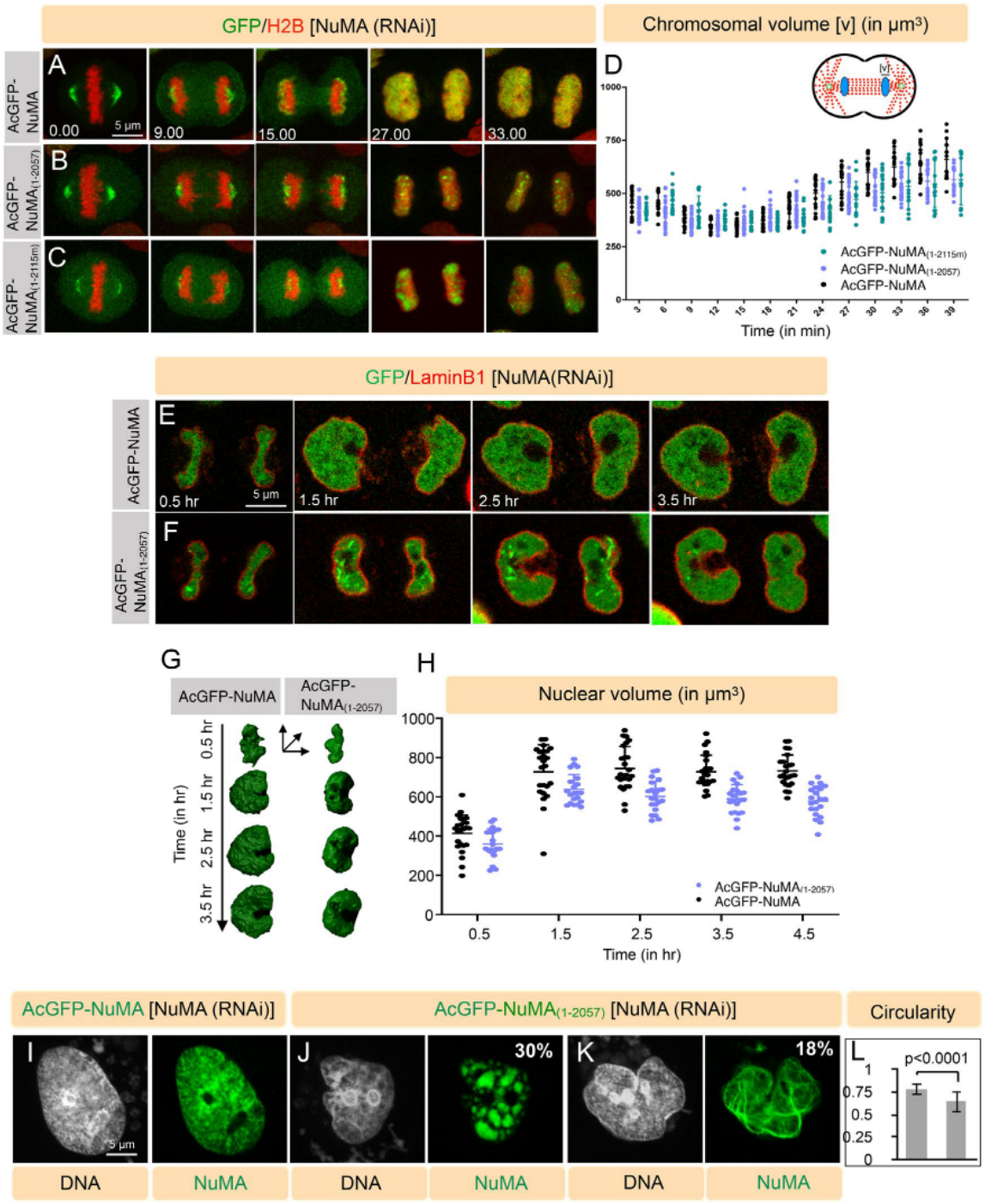

FIGURE 4: NuMA–DNA interaction is vital for DNA decompaction and proper nuclear architecture. (A–C) Images from the 4D-time-lapse confocal microscopy of HeLa cells stably expressing mCherry-H2B and depleted of endogenous NuMA by RNAi using siRNAs sequences targeting 3′UTR of NuMA (see the depletion efficiency of siRNAs in Figure 1B). These cells, as indicated, are transfected with AcGFP-NuMA (A), AcGFP-NuMA$_{(1–2057)}$ (B), or AcGFP-NuMA$_{(1–2115m)}$ (C). The GFP signal is shown in green, and the mCherry signal is in red. Time is indicated in minutes (min), time "0" min being the last frame of metaphase before the onset of chromosome segregation (also see corresponding Supplemental Movies S4–S6). (D) Schematic representation for the measurement of the chromosomal volume ([v] in µm^3) for the cells shown in A–C for 39 min post anaphase onset and their quantification. Note the significantly reduced chromosomal volume of cells expressing AcGFP-NuMA$_{(1–2057)}$ and AcGFP-NuMA$_{(1–2115m)}$ when compared with AcGFP-NuMA from 27 min onward ($p < 0.05$ from $t = 27$ min until $t = 39$ min for all data points between cells expressing AcGFP-NuMA and AcGFP-NuMA$_{(1–2057)}$ or AcGFP-NuMA$_{(1–2115m)}$). Statistical significance is calculated by two-tailed Student's t test ($n \geq 8$ cells; error bars: SD). (E, F) Images from the 4D-time-lapse confocal microscopy of HeLa Kyoto cells stably expressing mCherry-LaminB1 and depleted of endogenous NuMA by RNAi using siRNAs sequences targeting 3′UTR of NuMA. These cells, as indicated, are transfected with either AcGFP-NuMA (E) or AcGFP-NuMA$_{(1–2057)}$ (F). The GFP signal is shown in green and the mCherry signal in red. Time is indicated in hours (h), time "0" being the last frame of metaphase before the onset of chromosomes segregation. The images and the quantification for the nuclear volume (in panel H)

ensured that we are covering the entire nuclear volume by taking multiple optical sections using a confocal microscope. Live imaging (~9 h) in cells that were expressing full-length AcGFP-NuMA did not show any higher-order GFP-based structure (Figure 5A and Supplemental Movie S7). However, 24% of the cells expressing AcGFP-NuMA$_{(1–2057)}$ revealed a transition from a homogeneous soluble form to puncta formation, 14% of cells show a homogeneous soluble form to a fibrillar network, and 5% of cells formed fibrillar assemblies from puncta (Figure 5, B–D, and Supplemental Movies S8–S10). These analyses further revealed that these higher-order fibrillar or punctate structures observed upon AcGFP-NuMA$_{(1–2057)}$ expression were originated in the nucleus (Supplemental Figure S6A). Similarly, a 3D analysis of HeLa cells that were stably expressing mCherry-Lamin B1 and were transiently transfected with AcGFP-NuMA$_{(1–2057)}$ further revealed that these structures are primarily present inside the nucleus (Supplemental Figure S6B and Supplemental Movie S11). Next, we attempted to characterize the biophysical properties of punctate and fibrillar structures using FRAP. In comparison with the homogeneously soluble form of NuMA$_{(1–2057)}$ or NuMA$_{(1–2115m)}$ protein that exchanges rapidly in FRAP analysis as mentioned earlier for Figure 1, punctate structures observed with the expression of either of these mutated proteins were significantly slow in their recovery profile. Interestingly, the solid fibrillar networks that were found upon expression of these mutant proteins showed a much slower recovery profile, and a significantly smaller mobile fraction (Supplemental Figure S5, F–M).

These observations prompted us to test whether these higher-order solid fibrillar structures based on NuMA$_{(1–2057)}$ expression are capable of deforming the nucleus by mechanically pressing against the nuclear envelope. To this end, we conducted a live recording in HeLa cells that were stably expressing mCherry-Lamin B1 and were transiently transfected with AcGFP-NuMA$_{(1–2057)}$ and were also depleted for the endogenous NuMA protein. In this setting, we chose cells having a solid fibrillar network, and we analyzed the impact of such assemblies in the proximity of the nuclear envelope. Remarkably, these assemblies were capable of mechanically pressing against the nuclear envelope and thus efficient in causing nuclear deformation, as indicated by the absence of LaminB1 in deformed regions (Figure 5E). Overall, these sets of results suggest that the binding of NuMA to the DNA prevents higher-order NuMA assemblies comprising puncta and solid fibrillar networks, which are fatal for the nuclear architecture (see *Discussion*).

DISCUSSION

The accurate decondensation of the chromatin at the mitotic exit and the proper nuclear shape is essential to ensure appropriate gene regulation (Gerlich *et al.*, 2003; Baarlink *et al.*, 2017; Shoaib *et al.*, 2018; Kumar *et al.*, 2019). Recent studies have shown the involvement of PP1 phosphatase, PNUTS, and p97 AAA+ ATPase in chromosome decondensation during mitotic exit (Landsverk *et al.*, 2005; Ramadan *et al.*, 2007; reviewed in Antonin and Neumann, 2016). However, our knowledge related to the genes that are involved in the regulation of chromosome decondensation or nuclear shape remains limited. In this work, we have identified a novel contribution of a major mitotic regulator NuMA in orchestrating chromosome decondensation (Figure 6A) and nuclear shape (Figure 6B). Our model suggests that NuMA directly associates with the chromatin through the evolutionarily conserved sequences in its C-terminus, and this interaction ensures proper chromatin decondensation at the mitotic exit (Figure 6A).

NuMA interacts with chromatin in the interphase nucleus

Previously, NuMA was shown to remain in the insoluble fraction after DNase and high-salt treatment to the isolated nuclei, and thus it fulfilled the criteria of being categorized as a nuclear matrix component (Kallajoki *et al.*, 1991; Harborth *et al.*, 1995). Subsequently, biochemical analysis revealed that besides being part of the nuclear matrix, NuMA also interacts with chromatin (Abad *et al.*, 2007). In the last decade or so, several groups have linked NuMA's function in gene regulation. For instance, NuMA was shown to colocalize with a HMG I/Y and interact with putative transcription factors such as GAS41, and p53, and thus, it was suggested that NuMA might regulate gene expression (Harborth *et al.*, 2000; Tabellini *et al.*, 2001; Endo *et al.*, 2013; Ohata *et al.*, 2013). Furthermore, NuMA's nuclear function is linked to DNA repair (Vidi *et al.*, 2012, 2014; Salvador Moreno *et al.*, 2019). In this study, by conducting FRAP analysis in cells stably expressing AcGFP-NuMA, we revealed that the NuMA recovery profile ($t_{1/2}$) within the interphase nucleus is analogous to that of various transcription factors. Therefore, similar to the data obtained from an in vitro biochemical analysis, our data revealed that NuMA is not freely diffusing inside the nucleus of a living cell. Importantly, we have identified an evolutionarily conserved sequence at the C-terminus of NuMA that is critical for its direct interaction with the DNA, and thus chromatin. In the absence of DNA interaction, as in the case of mutant NuMA, its recovery rate ($t_{1/2}$) is much faster. What is the biological significance of NuMA's interaction with the DNA in the nucleus? Earlier work had suggested that NuMA could function as a nucleoskeletal component and may provide mechanical stability to the nucleus (Zeng *et al.*, 1994; Saredi *et al.*, 1996). Surprisingly, we did not observe any morphological defect related to the nuclear shape in cells that were having homogeneous distribution of the DNA-binding–deficient mutant of NuMA. These data indicate that NuMA–chromatin interaction may not serve a structural role in the nucleus, at least in the cell culture model. These results are consistent with the previous work where

were started at time 0.5 h post anaphase onset, when mCherry-LaminB1 significantly decorated the nuclear envelope after nuclear envelope reformation. (G) 3D surface reconstruction of daughter nuclei shown in panels E and F. 3D rendering was performed in Imaris (https://imaris.oxinst.com/) using AcGFP signal. (H) Quantification of the nuclear volume (in μm^3) for the cells shown in E and F (see *Materials and Methods*). Please note the significantly reduced nuclear volume for cells expressing AcGFP-NuMA$_{(1–2057)}$. $p < 0.05$ for $t = 0.5$ and 1.5 h, and $p < 0.0001$ for $t = 2.5$–4.5 h. Statistical significance is calculated by two-tailed Student's t test ($n \geq 10$; error bars: SD). (I–K) HeLa Kyoto cells in interphase are partly depleted of endogenous NuMA by RNAi using siRNAs sequences targeting 3'UTR of NuMA and transfected with AcGFP-NuMA (I) or AcGFP-NuMA$_{(1–2057)}$ (J, K). Cells were stained for GFP (green), and DNA is visualized in gray. Note the cells that express AcGFP-NuMA$_{(1–2057)}$ form puncta and fibrillar structure that are completely missing from cells expressing the wild-type form of NuMA (see also Supplemental Figure S5, A–E). Also, see the impact of AcGFP-NuMA$_{(1–2057)}$ expression on the nuclear shape. The percentage of cells showing puncta or fibrillar structure is indicated on the images. (L) Quantification of circularity (see *Materials and Methods*) of nuclei in cells expressing AcGFP-NuMA, or AcGFP-NuMA$_{(1–2057)}$ ($n = 70$ cells; error bars: SD).

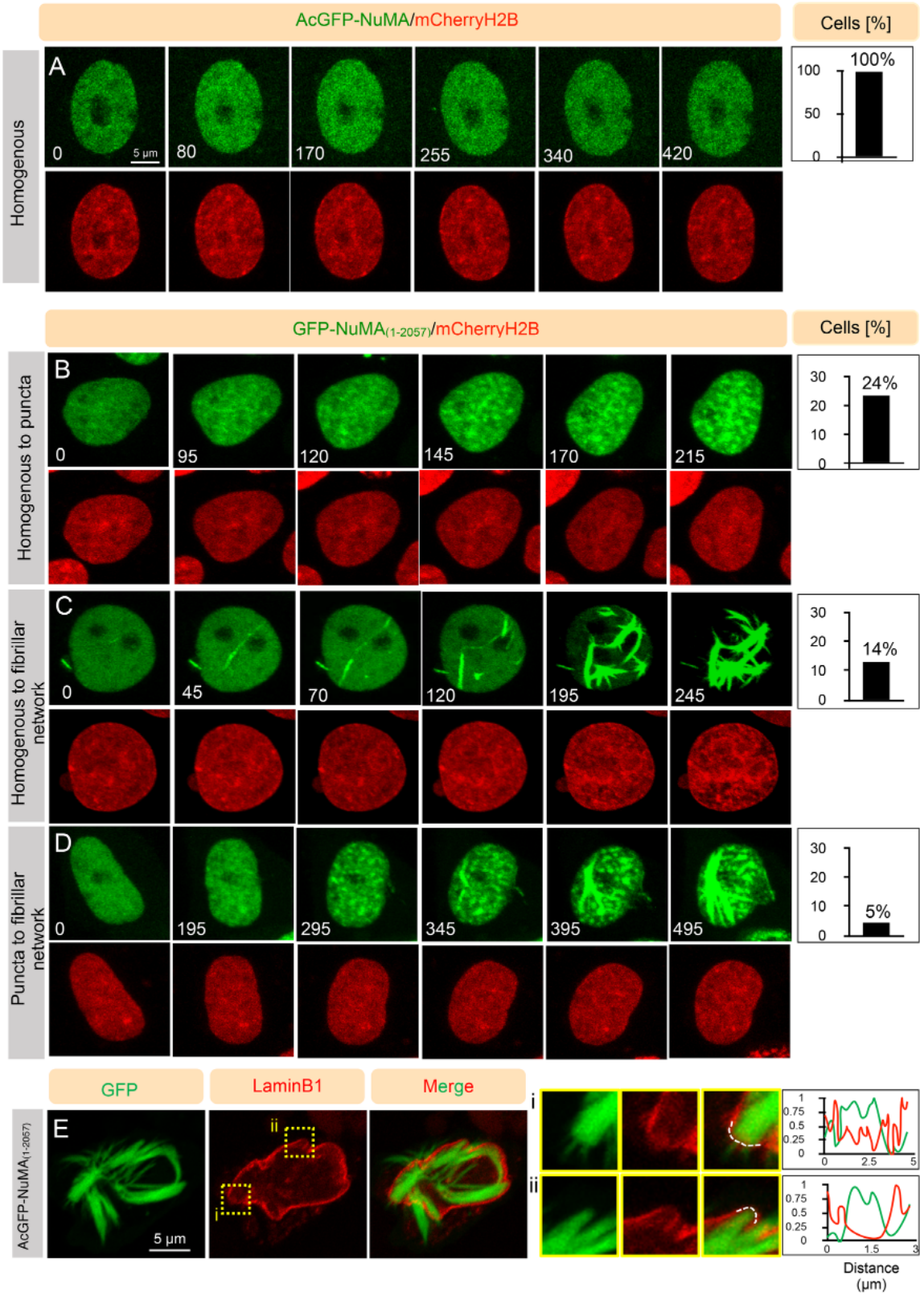

FIGURE 5: NuMA lacking the DNA-binding potential assembles into higher-order structures in the nucleus. (A) Images from the 4D-time-lapse confocal microscopy of HeLa cells stably expressing mCherry-H2B and transfected with AcGFP-NuMA. Time is indicated in minutes (min). Quantification on the right represents the percentage of cells that show homogeneous distribution of NuMA while conducting ~9 h of live recording ($n = 20$ cells). Also, see corresponding Supplemental Movie S7. (B–D) Images from the 4D-time-lapse confocal microscopy of HeLa cells stably expressing mCherry-H2B and transfected with AcGFP-NuMA$_{(1–2057)}$. The expression of AcGFP-NuMA$_{(1–2057)}$ leads to higher-order assemblies within the nucleus. These assemblies are categorized into three groups: homogeneous to puncta formation (B), homogeneous to the solid fibrillar network (C), or puncta to the solid fibrillar network (D). Quantification on the right

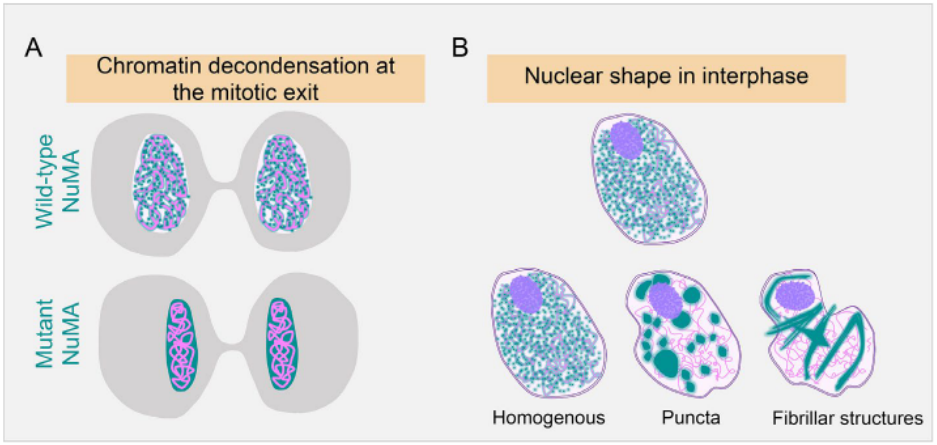

FIGURE 6: NuMA regulates DNA decondensation and nuclear shape via its ability to associate with chromatin. (A, B) Model for the NuMA function during mitotic exit (A) and in the interphase nuclei (B). In the control cells, wild-type NuMA interacts with chromatin during nuclear envelope reformation, and this allows proper chromatin decondensation in telophase/early G1 phase of the cell cycle. However, in cells that express DNA-binding–deficient mutant of NuMA, chromosomes mass in the newly formed daughter cells remains compact, and therefore the volume of the nucleus in the newly formed daughter cells remains significantly smaller (A). In the interphase this NuMA mutant exists in three different forms: homogeneous, puncta, and solid fibrillar network, and these higher-order assemblies, including puncta and solid fibrillar network, mechanically deform the nuclear architecture (B).

nuclei that were assembled using sperm DNA and *Xenopus* egg extracts depleted of NuMA did not lead to any morphological and functional errors in the nucleus (Merdes and Cleveland, 1998). The other exciting possibility could be that NuMA–DNA interaction may be crucial for providing mechanical stability to the nucleus within a tissue where cells are mechanically coupled with each other. Therefore, one interesting experiment would be to mechanically challenge cells in cultures that express the homogeneously distributed DNA-binding–deficient NuMA mutant to evaluate its function as a nucleoskeletal component.

NuMA–DNA interaction is critical for timely DNA decondensation

Remarkably, we noted that cells which express the DNA-binding–deficient mutant of NuMA show significant impairment in chromatin decondensation at the mitotic exit. How does NuMA promote chromatin decondensation? Previous work has shown that purified NuMA protein can assemble into multimeric oligomers (Gueth-Hallonet *et al.*, 1998; Harborth *et al.*, 1999). Also, overexpression of NuMA can lead to the formation of a three-dimensional quasihexagonal lattice in mammalian cells (Harborth *et al.*, 1999). Based on these observations, we hypothesize that the DNA-binding–deficient mutant of NuMA may not retain proper 3D organization, which might be necessary to keep the chromatin in a suitable configuration. Thus, in the absence of such association, chromatin remains tightly packaged (Figure 6A). While conducting long-term live-imaging experiments with the DNA-binding–deficient mutant of NuMA, we noted that cells that are in the early G1 phase show a significant impact on nuclear volume (Figure 4, E–H). However, we did not observe any errors related to the nuclear shape in cells expressing the homogeneously distributed mutant protein later in the cell cycle (unpublished data). One likely explanation for this observation is that the function of NuMA becomes redundant with other structural components within the nucleus as the cells progress beyond the G1 phase of the cell cycle. Nevertheless, assessing the impact of improper DNA decondensation on gene expression during early G1 phase in cells that express the DNA-binding–deficient mutant of NuMA would be of interest for future studies.

Cdk1 is critical for releasing NuMA from chromatin at mitotic entry

Our work demonstrated that Cdk1 activity helps in releasing NuMA from the chromatin in late prophase. This outcome could be because of the direct phosphorylation of NuMA by Cdk1, or an indirect consequence of Cdk1 phosphorylation on some other yet unknown protein. Because NuMA directly associates with the DNA in vitro, and C-terminus fragments of NuMA comprising the last 355 aa or smaller are efficient in binding to the chromosomes at all the mitotic stages, we favor the model that direct phosphorylation by Cdk1 dissociates NuMA from the chromosomes in mitosis. Unfortunately, mutation of all the Cdk1-phosphorylated residues mapped in several phosphoproteomics data one by one did not lead to the identification of a Cdk1-regulated residue(s) that is responsible for releasing NuMA from the chromatin. We envisage that this could be because more than one Cdk1-regulated residue is important in regulating NuMA-chromatin interaction.

DNA-binding–deficient mutant form of NuMA forms higher-order structures

Interestingly, a significant number of nuclei expressing the DNA-binding–defective mutant of NuMA showed higher-order assemblies into puncta and solid fibrillar networks. Also, the nuclei that carry these structures are improper in their architecture (Figure 6B). Notably, we uncovered that the solid fibrillar networks in these nuclei could mechanically deform the nucleus by compressing onto the nuclear membrane (Figure 6B). Moreover, our work revealed that these structures are not merely formed because of the overexpression of the mutant protein. We further ruled out the possibility that the nuclear architecture defects observed upon the DNA-binding–defective NuMA mutant are due to abnormal mitosis. The fibrillar

represents the percentage of cells that are grouped into these categories while conducting 9 h of live imaging ($n = 68$ cells). Also, see corresponding Supplemental Movies S8–S10. (E) Images from the time-lapse recording of HeLa Kyoto cells stably expressing mCherry-LaminB1 and transfected with AcGFP-NuMA$_{(1–2057)}$. The expression of AcGFP-NuMA$_{(1–2057)}$ leads to solid fibrillar networks. Insets of the areas (i and ii) are shown on the right with the line-scan intensity of mCherry-LaminB1 and of AcGFP-NuMA$_{(1–2057)}$ signal at the dashed white line covering a portion of the nuclear envelope. Note the decrease in the mCherry-LaminB1 intensity at those regions where AcGFP-NuMA$_{(1–2057)}$–based fibrillar networks are mechanically rupturing the nuclear envelope ($n > 10$ cells).

structures seen here seem reminiscent of what has been found in the cytoplasm by the expression of mutant NuMA lacking the NLS (Saredi *et al.*, 1996). Thus, it is tempting to speculate that the ΔNLS mutant of NuMA is capable of forming such an extensive network as they lack interaction with the DNA, which would otherwise block NuMA's ability to make such extensive network structures.

Moreover, the punctate structures that we have described in cells expressing the DNA-binding–deficient mutant of NuMA were also reported in apoptotic and virus-infected cells where NuMA was found to be cleaved at its C-terminus (Hsu and Yeh, 1996; Sodja *et al.*, 1997; Taimen and Kallajoki, 2003; Taimen *et al.*, 2004). These punctate structures found in apoptotic cells could be due to NuMA's inability to interact with DNA due to truncation at the C-terminus. Therefore, establishing whether the presence of these structures in the apoptotic cells is because of the perturbed NuMA–DNA interaction would be a next logical step to further evaluate the function of this important molecule.

Overall, this work unveiled yet another critical function of NuMA in regulating chromatin decondensation during the cell cycle by directly associating with DNA.

MATERIALS AND METHODS

Cell culture, plasmid, and siRNAs transfection, and stable cell line generation

All the cell lines that were used in this study were cultured in high-glucose DMEM with GlutaMAX (CC3004; Genetix) supplemented with 10% fetal calf serum in a humidified 5% CO_2 incubator at 37°C. For plasmid transfections, cells were seeded at 80% confluency in an imaging dish (0030740017; Eppendorf) or on coverslips in six-well plates. Plasmid DNA (4 µg) suspended in 400 µl of serum-free DMEM was incubated for 5 min, followed by the addition of 6 µl of lipofectamine 2000 (11668019; Life Technologies) or 6 µl turbofect (R0531; ThermoFisher Scientific), and was mixed and incubated for 15 min. This mixture was then added to the cells, and the cells were fixed or imaged 30–36 h posttransfection.

For the siRNA experiment, 6 or 9 µl of 20 µM siRNA and 4 µl of lipofectamine RNAi MAX (13778150, Invitrogen) were suspended in 100 µl of water (W4502; Sigma) and were incubated for 5 min in parallel, then mixed and incubated for another 15 min. This mixture was added to the 2.5 ml medium per well containing around 100,000 cells. Cells were then grown for 60–72 h before fixation or live imaging.

The protocol for generating stable HeLa Kyoto cells stably expressing AcGFP-NuMA was described recently (Keshri *et al.*, 2020). For the generation of stable cells expressing mCherry-LaminB1 in HeLa Kyoto, cells were cultured in a 10-cm dish at 80% confluency. These cells were then transfected with 6 µg of pIRES-mCherry-LaminB1 plasmid using 12 µl of lipofectamine. After 36 h, 400 ng/µl puromycin media was added for the selection. Isolated colonies were cultured, and clones were confirmed by immunostaining and immunoblot analysis.

Plasmids and siRNAs

All NuMA clones were amplified from a previously existing plasmid as a template with appropriate PCR primer pairs. NuMA full-length and $NuMA_{(1–2057)}$ was cloned into a pIRES-AcGFP-FLAG plasmid (a gift from Mark Petronczki) using *Age*1 and *Eco*R1 sites. For cloning $NuMA_{(1–2115m)}$, the *Kpn*2I site was introduced in pIRES-AcGFP-NuMA plasmid and custom-made double-stranded DNA (from Macrogen, Inc.) where all the arginine and lysine residues from 2058–2115 are converted to alanine was cloned using *Kpn*2I and *Eco*R1 sites. pIRES-NLS-AcGFP plasmid was cloned by incorporating the SV-40 NLS sequence into the forward primer used for amplifying AcGFP. All the smaller C-terminus fragments of NuMA were cloned in pcDNA3-GFP vector (Merdes *et al.*, 2000) using the Xba1 and Not1 sites. All Cdk1 phosphorylated residues (threonine or serine) in NuMA were mutated using the megaprimer approach. For recombinant protein expression in *E. coli*, $NuMA_{(2058–2115)}$, $NuMA_{(1877–2115)}$, and $NuMA_{(1877–2057)}$ were cloned in pET30a plasmid with a hexahistidine tag at the N-terminus using the *Nco*1 and *Eco*R1 sites. Bacteria histone-like HU protein was generously provided by V. Nagaraja (MCB, IISc).

Double-stranded siRNA oligonucleotides used were 5′- CAGUACCAGUGAGUGGCCCCACCUG-3′ (NuMA 3′UTR siRNA; Eurogentec) and 5′-CACCGUGUGUCUAAGCAAA-3′ (RCC1 siRNA; Eurogentec).

Drug-mediated inhibition of mitotic kinases

hTERT-RPE1 cells were synchronized in early prophase by a double-thymidine block. Briefly, the cells were treated with 2 mM thymidine (T1895; Sigma-Aldrich) for 17 h, then released for 8 h followed by another round of thymidine treatment. Following thymidine release, cells were treated with dimethyl sulfoxide (DMSO) for control, 20 µM or 100 µM of Cdk1 inhibitor RO-3306 (S7747; Selleckchem) for 10 min, 250 nM or 1.25 µM of Aurora A inhibitor MLN-8054 (S1100; Selleckchem) for 1 h, and 300 nM or 1.5 µM of Plk1 inhibitor BI-2536 (S1109; Selleckchem) for 30 min before fixation. Following treatment with the inhibitors, cells were fixed with cold methanol and immunostained with antibodies against NuMA (sc-48773; Santa Cruz) and γ-tubulin (GTU88; Sigma-Aldrich).

Time-lapse imaging and FRAP analysis

Time-lapse microscopy was conducted on an Olympus FV 3000 confocal laser scanning microscope using a 40× (NA 1.3) oil immersion objective (Olympus Corporation, Japan) using an imaging dish (0030740017; Eppendorf) at 5% CO_2, 37°C, 90% humidity maintained by a Tokai Hit STR Stage Top incubator with touch panel controller. For mitotic cells, images were acquired at the interval of either 2 min or 3 min with 9–11 optical sections (3 µm apart). For the interphase cells, images were captured every 5 min with optical sectioning of either 1 µm or 0.3 µm without conducting time-lapse.

FRAP experiments were performed for a specific region (1.75 μm^2) of the nucleus of HeLa cells stably expressing AcGFP-NuMA, or cells that are transiently transfected with AcGFP-$NuMA_{(1–2057)}$, AcGFP-$NuMA_{(1–2115m)}$, or AcGFP-NLS with a 40× objective. Forty percent of the 488-nm laser was utilized to bleach the region of interest, and images within the same focal plane were acquired every 5 s for the entire duration of 50 cycles to monitor fluorescence recovery. Due to faster recovery in cells that are expressing AcGFP-$NuMA_{(1–2057)}$, AcGFP-$NuMA_{(1–2115m)}$, or AcGFP-NLS, images were acquired every 2 s. To assess the fluorescence loss due to photobleaching, fluorescence from a region separated from the bleached region was simultaneously recorded. The intensity value in the bleached area was measured, corrected for the background, and the curves were then normalized using the following equation:

$$I = (I_t - I_{\min}) / (I_{\max} - I_{\min})$$

where I represents the normalized intensity, I_t represents the intensity at a time point, $I_{\min}$ is the minimum intensity (at the time of bleaching), and $I_{\max}$ is the maximum intensity (prebleaching intensity). For the calculation of half-time of recovery ($t_{1/2}$) or mobile fraction, the bleaching due to imaging was considered, and the values were quantified by fitting to a first-order exponential equation using the Origin software (https://www.originlab.com/origin).

Nuclear fractionation

To obtain the nuclear matrix or chromosomal fraction, we utilized a method as described in Abad et al., 2007. In brief, HeLa Kyoto cells washed with phosphate-buffered saline (PBS) –protease inhibitors (PIs; Merck; Cat. no. 539134) and were collected at 450 × *g* at 4°C for 5 min and were suspended in 1 ml of buffer A (10 mM HEPES, pH 7.4, 1 mM EGTA, 2 mM $MgCl_2$, 250 mM sucrose, and PI). After that, 1 ml of buffer B (1 mM HEPES, pH 7.4, containing PI) was added and was incubated on ice for 30 min. Separation of nuclei from the cytoplasm was performed using a Dounce homogenizer, and this was confirmed under an epifluorescence microscope using Hoechst 33342 (B2261; Sigma-Aldrich). The nuclear pellet was collected at 3200 × *g* at 4°C for 15 min and was suspended in buffer X (10 mM HEPES, pH 7.9, 10 mM KCl, 1.5 mM $MgCl_2$, 0.34 M sucrose, 10% (vol/vol) glycerol, 1 mM dithiothreitol, and PI) with Triton X-100 0.1% (vol/vol), and was incubated on ice for 8 min, and pelleted down at 1300 × *g* at 4°C for 5 min. The pellet was washed again with buffer X. Nuclei were lysed in buffer Y (3 mM EDTA, 0.2 mM EGTA, 1 mM dithiothreitol, and PI) on ice for 30 min. The pellet formed at 1650 × *g* at 4°C for 5 min was rewashed with buffer Y. The pellet was subjected to 0.1 µl Mnase (EN0181; Fermentas) in 100 µl of MNase buffer (10 mM Tris, pH 8.8, 10 mM KCl, and 1 mM $CaCl_2$) at 37°C for 15 min. The reaction was stopped using 1 mM EGTA. The nuclease-sensitive, chromatin fraction (CF) and the resistant matrix fraction (MF) were separated by at 1650 × *g* at 4°C for 5min. The MF was washed with 100 µl of MNase buffer. CF and MF were suspended in Laemmli buffer and denatured at 99°C for 10 min, and then utilized for immunoblotting.

Higher-resolution imaging

Higher-resolution imaging was conducted on an Olympus spinning disk superresolution confocal microscope (IXplore SpinSR) using a 100× (1.45 NA) objective. Images were acquired by capturing 13 Z-sections, 0.23 µm apart. The images were processed with Olympus Super Resolution software.

Electrophoretic mobility shift assay

Recombinant protein HU, $NuMA_{(2058–2115)}$, $NuMA_{(1877–2115)}$, $NuMA_{(1877–2057)}$, or NuMA-N ter(1–705) was incubated with 400 ng of pUC19 plasmid in 1×-TAE (89 mM tris, 89 mM acetic acid, 1 mM EDTA, pH 8.4) buffer at 27°C for 30 min. The protein–DNA complexes were resolved in 4% acrylamide gel in 1×-TAE buffer. The gel was stained with ethidium bromide and visualized under UV light.

Indirect immunofluorescence and immunoblotting

For immunofluorescence, cells were fixed with chilled methanol at –20°C for 10 min and washed in PBST (PBS containing 0.05% Triton X-100). Cells were blocked in 1% bovine serum albumin (RM3159; HiMedia) for 1 h, followed by incubation with primary antibody for 4 h at room temperature. After three washes of 5 min each with PBST, cells were incubated with secondary antibody for 1 h. Cells were then given three washes with PBST and stained with 1 µg/ml Hoechst 33342 (B2261; Sigma-Aldrich) for 5 min. Following three washes with PBST, the coverslips were mounted using Fluoromount (Southern-Biotech; 0100-01). The primary antibodies used were 1:1000 mouse anti-GFP (2955S; Cell Signaling Technology), 1:200 rabbit anti-NuMA (sc-48773; Santa Cruz), 1:200 mouse anti-RCC1 (sc-376049; Santa Cruz), 1:1000 mouse anti–γ-tubulin (GTU88; Sigma-Aldrich), and 1:200 rabbit anti-Ect2 (07-1364; Merck). Secondary antibodies used were 1:500 Alexa Fluor 488 goat anti-mouse (A11001; Invitrogen), 1:500 Alexa Fluor 488 goat anti-rabbit (A11008; Invitrogen), 1:500 Alexa Fluor 568 goat anti-mouse (A11004; Invitrogen), and 1:500 Alexa Fluor 568 goat anti-rabbit (A11011; Invitrogen). Confocal images were acquired on an Olympus FV 3000 confocal laser scanning microscope using a 60× (NA 1.4) oil immersion objective. All the images are processed in ImageJ.

For immunoblotting, HeLa Kyoto cells or HeLa Kyoto cells transfected with NuMA siRNAs against 3'UTR or HeLa Kyoto cells stably expressing AcGFP-NuMA were synchronized in prometaphase with 100 nM Nocodazole (M1404; Sigma-Aldrich) for 20 h. Cells were lysed in lysis buffer (50 mM Tris, pH 7.4, 150 mM NaCl, 2 mM EDTA, 2 mM EGTA, 25 mM sodium fluoride, 0.1 mM sodium orthovanadate, 0.1 mM phenylmethylsulfonyl fluoride, 0.2% Triton X-100, 0.3% NP-40, 100 nM Okadaic acid, and complete EDTA-free protease inhibitor) for 2 h on ice and after a spin of 14,000 rpm, cell supernatant was denatured at 99°C in 2× SDS–PAGE buffer and analyzed by SDS–PAGE followed by immunoblotting. For immunoblotting, 1:1000 rabbit anti-NuMA (sc-48773; Santa Cruz), 1:5000 mouse anti-actin (sc-58673; Santa Cruz), 1:1000 of mouse anti-LaminB1 (sc-6216; Santa Cruz), and rabbit anti-RNA polymerase A (sc-899; Santa Cruz) antibodies were used.

Quantifications and statistical analysis

All quantifications were performed in ImageJ. Quantification of GFP chromosomal intensity was determined by calculating the ratio of mean chromosomal intensity and mean cytoplasmic intensity (of a rectangular region of interest of area 1.69 μm^2) and correcting for the background signal.

The volume of the segregated chromosomal mass at anaphase onset was estimated as the cumulative integral of the area multiplied by the voxel depth in ImageJ. For Figure 4D, the area was calculated by thresholding the mCherry-H2B signal using the ImageJ "3D-Object counter" plugin (https://imagej.net/3D_Objects_Counter). To use this plugin for computation of volume in a time series, a custom-written macro on ImageJ was used to loop through the time-lapse images, and the threshold value for the plugin was fixed at 230. This threshold number was judged to be optimally suited for all z-stacks in the time-lapse confocal images by visual inspection. To validate the results of the volume analysis from this plugin, image thresholding was performed, and the area was manually traced in each z-stack. Comparable results were obtained from this analysis. This procedure was also used for nuclear volume measurements in Figure 4H. The freehand tool on ImageJ was used for accurately outlining the nuclear periphery (defined by the mCherry-LaminB1 signal) and the area in each z-stack for a single time frame. Volume measurement is the summation of the area from the z-stacks, multiplied by the voxel depth.

The circularity of the nucleus was calculated using the freehand tool to manually select the outline of the nucleus, and circularity was calculated using the formula $4\pi(\text{area}/\text{perimeter}^2)$.

Spindle pole enrichment of NuMA was determined by calculating the ratio of mean spindle pole intensity and mean cytoplasmic intensity after correcting for background signal, as described in Sana *et al.*, 2018.

Midzone Ect2 intensity was measured using a rectangular region of interest of 1.09 μm^2 and was corrected for background signal.

Whole-cell GFP intensity was measured using the freehand tool in ImageJ to select the outline of the nucleus. To rule out the difference in nuclear area of individual cells, the intensity was divided by the total area used for quantification to obtain intensity/μm^2.

Supplemental Movies S1–S10 were made in ImageJ using images from the time-lapse confocal microscopy, and Supplemental Movie S11 was made in Imaris (Bitplane) using 3D images from the confocal microscope with an optical sectioning of 0.3 µm.

To calculate the significance of the differences between two mean values, two-tailed Student's *t* tests were performed. A *p* value was considered to be significant if $p \leq 0.05$ using GraphPad Prism 8.

ACKNOWLEDGMENTS

We are grateful to Sophie Dumont and Andrea Serra-Marques for sharing with us their unpublished data, and for the fruitful discussions. We thank Andreas Merdes, Arnaud Echard, Mark Petronczki, V. Nagaraja, Daniel Gerlich, and Anthony Hyman for providing us plasmids, recombinant protein, and cell lines. We thank Phong Tran, Raj Ladher, Sveta Chakrabarti, and Fernando R. Balestra for providing us with critical comments on the manuscript. We thank Ganesh Kadasoor (Olympus Corporation) for taking higher-resolution confocal images on the Olympus IXplore SpinSR microscope system. We thank DST-FIST, UGC Centre for the Advanced Study, DBT-IISc Partnership Program, and IISc for the infrastructure support. This work is supported by a grant from the Wellcome Trust DBT-India Alliance (Grant no. IA/I/15/2/502077) to S.K. S.K. is a Wellcome Trust DBT-India Alliance Intermediate Fellow.

REFERENCES

Abad PC, Lewis J, Mian IS, Knowles DW, Sturgis J, Badve S, Xie J, Lelievre SA (2007). NuMA influences higher order chromatin organization in human mammary epithelium. Mol Biol Cell 18, 348–361.

Antonin W, Neumann H (2016). Chromosome condensation and decondensation during mitosis. Curr Opin Cell Biol 40, 15–22.

Baarlink C, Plessner M, Sherrard A, Morita K, Misu S, Virant D, Kleinschnitz EM, Harniman R, Alibhai D, Baumeister S, et al. (2017). A transient pool of nuclear F-actin at mitotic exit controls chromatin organization. Nat Cell Biol 19, 1389–1399.

Batty P, Gerlich DW (2019). Mitotic chromosome mechanics: how cells segregate their genome. Trends Cell Biol 29, 717–726.

Chandramouly G, Abad PC, Knowles DW, Lelièvre SA (2007). The control of tissue architecture over nuclear organization is crucial for epithelial cell fate. J Cell Sci 120, 1596–1606.

Cleveland DW (1995). NuMA: a protein involved in nuclear structure, spindle assembly, and nuclear re-formation. Trends Cell Biol 5, 60–64.

Compton DA, Cleveland DW (1993). NuMA is required for the proper completion of mitosis. J Cell Biol 120, 947–957.

Compton DA, Szilak I, Cleveland DW (1992). Primary structure of NuMA, an intranuclear protein that defines a novel pathway for segregation of proteins at mitosis. J Cell Biol 116, 1395–1408.

Cuijpers SAG, Vertegaal ACO (2018). Guiding mitotic progression by crosstalk between post-translational modifications. Trends Biochem Sci 43, 251–268.

Das AT, Luderus ME, Lamers WH (1993). Identification and analysis of a matrix-attachment region 5′ of the rat glutamate-dehydrogenase-encoding gene. Eur J Biochem 215, 777–785.

Dephoure N, Zhou C, Villen J, Beausoleil SA, Bakalarski CE, Elledge SJ, Gygi SP (2008). A quantitative atlas of mitotic phosphorylation. Proc Natl Acad Sci USA 105, 10762–10767.

Du Q, Macara IG (2004). Mammalian Pins is a conformational switch that links NuMA to heterotrimeric G proteins. Cell 119, 503–516.

Endo A, Moyori A, Kobayashi A, Wong RW (2013). Nuclear mitotic apparatus protein, NuMA, modulates p53-mediated transcription in cancer cells. Cell Death Dis 4, e713.

Finn EH, Pegoraro G, Brandao HB, Valton AL, Oomen ME, Dekker J, Mirny L, Misteli T (2019). Extensive heterogeneity and intrinsic variation in spatial genome organization. Cell 176, 1502–1515.e1510.

Friedl P, Wolf K, Lammerding J (2011). Nuclear mechanics during cell migration. Curr Opin Cell Biol 23, 55–64.

Gerlich D, Beaudouin J, Kalbfuss B, Daigle N, Eils R, Ellenberg J (2003). Global chromosome positions are transmitted through mitosis in mammalian cells. Cell 112, 751–764.

Gueth-Hallonet C, Wang J, Harborth J, Weber K, Osborn M (1998). Induction of a regular nuclear lattice by overexpression of NuMA. Exp Cell Res 243, 434–452.

Hager GL, McNally JG, Misteli T (2009). Transcription dynamics. Mol Cell 35, 741–753.

Harborth J, Wang J, Gueth-Hallonet C, Weber K, Osborn M (1999). Self assembly of NuMA: multiarm oligomers as structural units of a nuclear lattice. EMBO J 18, 1689–1700.

Harborth J, Weber K, Osborn M (1995). Epitope mapping and direct visualization of the parallel, in-register arrangement of the double-stranded coiled-coil in the NuMA protein. EMBO J 14, 2447–2460.

Harborth J, Weber K, Osborn M (2000). GAS41, a highly conserved protein in eukaryotic nuclei, binds to NuMA. J Biol Chem 275, 31979–31985.

Hoar K, Chakravarty A, Rabino C, Wysong D, Bowman D, Roy N, Ecsedy JA (2007). MLN8054, a small-molecule inhibitor of Aurora A, causes spindle pole and chromosome congression defects leading to aneuploidy. Mol Cell Biol 27, 4513–4525.

Houtsmuller AB (2005). Fluorescence recovery after photobleaching: application to nuclear proteins. Adv Biochem Eng Biotechnol 95, 177–199.

Hsu HL, Yeh NH (1996). Dynamic changes of NuMA during the cell cycle and possible appearance of a truncated form of NuMA during apoptosis. J Cell Sci 109 (Pt 2), 277–288.

Hueschen CL, Galstyan V, Amouzgar M, Phillips R, Dumont S (2019). Microtubule end-clustering maintains a steady-state spindle shape. Curr Biol 29, 700–708.e705.

Jayaraman S, Chittiboyina S, Bai Y, Abad PC, Vidi PA, Stauffacher CV, Lelièvre SA (2017). The nuclear mitotic apparatus protein NuMA controls rDNA transcription and mediates the nucleolar stress response in a p53-independent manner. Nucleic Acids Res 45, 11725–11742.

Kallajoki M, Harborth J, Weber K, Osborn M (1993). Microinjection of a monoclonal antibody against SPN antigen, now identified by peptide sequences as the NuMA protein, induces micronuclei in PtK2 cells. J Cell Sci 104 (Pt 1), 139–150.

Kallajoki M, Weber K, Osborn M (1991). A 210 kDa nuclear matrix protein is a functional part of the mitotic spindle; a microinjection study using SPN monoclonal antibodies. EMBO J 10, 3351–3362.

Kallajoki M, Weber K, Osborn M (1992). Ability to organize microtubules in taxol-treated mitotic PtK2 cells goes with the SPN antigen and not with the centrosome. J Cell Sci 102 (Pt 1), 91–102.

Keshri R, Rajeevan A, Kotak S (2020). PP2A-B55γ counteracts Cdk1 and regulates proper spindle orientation through the cortical dynein adaptor NuMA. J Cell Sci 133, jcs243857.

Kiyomitsu T, Cheeseman IM (2012). Chromosome- and spindle-pole-derived signals generate an intrinsic code for spindle position and orientation. Nat Cell Biol 14, 311–317.

Kotak S, Afshar K, Busso C, Gonczy P (2016). Aurora A kinase regulates proper spindle positioning in *C. elegans* and in human cells. J Cell Sci 129, 3015–3025.

Kotak S, Busso C, Gonczy P (2012). Cortical dynein is critical for proper spindle positioning in human cells. J Cell Biol 199, 97–110.

Kotak S, Busso C, Gonczy P (2013). NuMA phosphorylation by CDK1 couples mitotic progression with cortical dynein function. EMBO J 32, 2517–2529.

Kotak S, Busso C, Gonczy P (2014). NuMA interacts with phosphoinositides and links the mitotic spindle with the plasma membrane. EMBO J 33, 1815–1830.

Kumar R, Lizana L, Stenberg P (2019). Genomic 3D compartments emerge from unfolding mitotic chromosomes. Chromosoma 128, 15–20.

Lammerding J, Schulze PC, Takahashi T, Kozlov S, Sullivan T, Kamm RD, Stewart CL, Lee RT (2004). Lamin A/C deficiency causes defective nuclear mechanics and mechanotransduction. J Clin Invest 113, 370–378.

Landsverk HB, Kirkhus M, Bollen M, Küntziger T, Collas P (2005). PNUTS enhances in vitro chromosome decondensation in a PP1-dependent manner. Biochem J 390, 709–717.

Lindqvist A, Rodriguez-Bravo V, Medema RH (2009). The decision to enter mitosis: feedback and redundancy in the mitotic entry network. J Cell Biol 185, 193–202.

Lydersen BK, Pettijohn DE (1980). Human-specific nuclear protein that associates with the polar region of the mitotic apparatus: distribution in a human/hamster hybrid cell. Cell 22, 489–499.

Merdes A, Cleveland DW (1998). The role of NuMA in the interphase nucleus. J Cell Sci 111 (Pt 1), 71–79.

Merdes A, Heald R, Samejima K, Earnshaw WC, Cleveland DW (2000). Formation of spindle poles by dynein/dynactin-dependent transport of NuMA. J Cell Biol 149, 851–862.

Merdes A, Ramyar K, Vechio JD, Cleveland DW (1996). A complex of NuMA and cytoplasmic dynein is essential for mitotic spindle assembly. Cell 87, 447–458.

Mirny LA, Imakaev M, Abdennur N (2019). Two major mechanisms of chromosome organization. Curr Opin Cell Biol 58, 142–152.

Nagano T, Lubling Y, Varnai C, Dudley C, Leung W, Baran Y, Mendelson Cohen N, Wingett S, Fraser P, Tanay A (2017). Cell-cycle dynamics of chromosomal organization at single-cell resolution. Nature 547, 61–67.

Nishimoto T, Eilen E, Basilico C (1978). Premature chromosome condensation in a ts DNA-mutant of BHK cells. Cell 15, 475–483.
Nishitani H, Ohtsubo M, Yamashita K, Iida H, Pines J, Yasudo H, Shibata Y, Hunter T, Nishimoto T (1991). Loss of RCC1, a nuclear DNA-binding protein, uncouples the completion of DNA replication from the activation of cdc2 protein kinase and mitosis. EMBO J 10, 1555–1564.
Nozaki T, Imai R, Tanbo M, Nagashima R, Tamura S, Tani T, Joti Y, Tomita M, Hibino K, Kanemaki MT, et al. (2017). Dynamic organization of chromatin domains revealed by super-resolution live-cell imaging. Mol Cell 67, 282–293.e287.
Ohata H, Miyazaki M, Otomo R, Matsushima-Hibiya Y, Otsubo C, Nagase T, Arakawa H, Yokota J, Nakagama H, Taya Y, Enari M (2013). NuMA is required for the selective induction of p53 target genes. Mol Cell Biol 33, 2447–2457.
Petronczki M, Glotzer M, Kraut N, Peters JM (2007). Polo-like kinase 1 triggers the initiation of cytokinesis in human cells by promoting recruitment of the RhoGEF Ect2 to the central spindle. Dev Cell 12, 713–725.
Petrone A, Adamo ME, Cheng C, Kettenbach AN (2016). Identification of candidate cyclin-dependent kinase 1 (Cdk1) substrates in mitosis by quantitative phosphoproteomics. Mol Cell Proteomics 15, 2448–2461.
Price CM, Pettijohn DE (1986). Redistribution of the nuclear mitotic apparatus protein (NuMA) during mitosis and nuclear assembly. Properties of purified NuMA protein. Exp Cell Res 166, 295–311.
Qian J, Lesage B, Beullens M, Van Eynde A, Bollen M (2011). PP1/Repoman dephosphorylates mitotic histone H3 at T3 and regulates chromosomal aurora B targeting. Curr Biol 21, 766–773.
Radulescu AE, Cleveland DW (2010). NuMA after 30 years: the matrix revisited. Trends Cell Biol 20, 214–222.
Ramadan K, Bruderer R, Spiga FM, Popp O, Baur T, Gotta M, Meyer HH (2007). Cdc48/p97 promotes reformation of the nucleus by extracting the kinase Aurora B from chromatin. Nature 450, 1258–1262.
Rogers S, McCloy RA, Parker BL, Chaudhuri R, Gayevskiy V, Hoffman NJ, Watkins DN, Daly RJ, James DE, Burgess A (2015). Dataset from the global phosphoproteomic mapping of early mitotic exit in human cells. Data Brief 5, 45–52.
Salvador Moreno N, Liu J, Haas KM, Parker LL, Chakraborty C, Kron SJ, Hodges K, Miller LD, Langefeld C, Robinson PJ, et al. (2019). The nuclear structural protein NuMA is a negative regulator of 53BP1 in DNA double-strand break repair. Nucleic Acids Res 47, 2703–2715.
Sana S, Keshri R, Rajeevan A, Kapoor S, Kotak S (2018). Plk1 regulates spindle orientation by phosphorylating NuMA in human cells. Life Sci Alliance 1, e201800223.
Saredi A, Howard L, Compton DA (1996). NuMA assembles into an extensive filamentous structure when expressed in the cell cytoplasm. J Cell Sci 109 (Pt 3), 619–630.
Seldin L, Poulson ND, Foote HP, Lechler T (2013). NuMA localization, stability, and function in spindle orientation involve 4.1 and Cdk1 interactions. Mol Biol Cell 24, 3651–3662.
Shoaib M, Nair N, Sørensen CS (2020). Chromatin landscaping at mitotic exit orchestrates genome function. Front Genet 11, 103.
Shoaib M, Walter D, Gillespie PJ, Izard F, Fahrenkrog B, Lleres D, Lerdrup M, Johansen JV, Hansen K, Julien E, et al. (2018). Histone H4K20 methylation mediated chromatin compaction threshold ensures genome integrity by limiting DNA replication licensing. Nat Commun 9, 3704.
Sodja C, Walker PR, Brown DL, Chaly N (1997). Unique behaviour of NuMA during heat-induced apoptosis of lymphocytes. Biochem Cell Biol 75, 399–414.
Steegmaier M, Hoffmann M, Baum A, Lenart P, Petronczki M, Krssak M, Gurtler U, Garin-Chesa P, Lieb S, Quant J, et al. (2007). BI 2536, a potent and selective inhibitor of polo-like kinase 1, inhibits tumor growth in vivo. Curr Biol 17, 316–322.
Tabellini G, Riccio M, Baldini G, Bareggi R, Billi AM, Grill V, Narducci P, Martelli AM (2001). Further considerations on the intranuclear distribution of HMGI/Y proteins. Ital J Anat Embryol 106, 251–260.
Taimen P, Berghäll H, Vainionpää R, Kallajoki M (2004). NuMA and nuclear lamins are cleaved during viral infection—inhibition of caspase activity prevents cleavage and rescues HeLa cells from measles virus-induced but not from rhinovirus 1B-induced cell death. Virology 320, 85–98.
Taimen P, Kallajoki M (2003). NuMA and nuclear lamins behave differently in Fas-mediated apoptosis. J Cell Sci 116, 571–583.
Tang TK, Tang CJ, Chen YL, Wu CW (1993). Nuclear proteins of the bovine esophageal epithelium. II. The NuMA gene gives rise to multiple mRNAs and gene products reactive with monoclonal antibody W1. J Cell Sci 104 (Pt 2), 249–260.
Vagnarelli P, Ribeiro S, Sennels L, Sanchez-Pulido L, de Lima Alves F, Verheyen T, Kelly DA, Ponting CP, Rappsilber J, Earnshaw WC (2011). Repo-Man coordinates chromosomal reorganization with nuclear envelope reassembly during mitotic exit. Dev Cell 21, 328–342.
Van Steensel B, Belmont AS (2017). Lamina-associated domains: links with chromosome architecture, heterochromatin, and gene repression. Cell 169, 780–791.
Vassilev LT, Tovar C, Chen S, Knezevic D, Zhao X, Sun H, Heimbrook DC, Chen L (2006). Selective small-molecule inhibitor reveals critical mitotic functions of human CDK1. Proc Natl Acad Sci USA 103, 10660–10665.
Vidi PA, Chandramouly G, Gray M, Wang L, Liu E, Kim JJ, Roukos V, Bissell MJ, Moghe PV, Lelièvre SA (2012). Interconnected contribution of tissue morphogenesis and the nuclear protein NuMA to the DNA damage response. J Cell Sci 125, 350–361.
Vidi PA, Liu J, Salles D, Jayaraman S, Dorfman G, Gray M, Abad P, Moghe PV, Irudayaraj JM, Wiesmüller L, Lelièvre SA (2014). NuMA promotes homologous recombination repair by regulating the accumulation of the ISWI ATPase SNF2h at DNA breaks. Nucleic Acids Res 42, 6365–6379.
Wandke C, Kutay U (2013). Enclosing chromatin: reassembly of the nucleus after open mitosis. Cell 152, 1222–1225.
Woodard GE, Huang NN, Cho H, Miki T, Tall GG, Kehrl JH (2010). Ric-8A and Giα recruit LGN, NuMA, and dynein to the cell cortex to help orient the mitotic spindle. Mol Cell Biol 30, 3519–3530.
Yang CH, Lambie EJ, Snyder M (1992). NuMA: an unusually long coiled-coil related protein in the mammalian nucleus. J Cell Biol 116, 1303–1317.
Yang CH, Snyder M (1992). The nuclear-mitotic apparatus protein is important in the establishment and maintenance of the bipolar mitotic spindle apparatus. Mol Biol Cell 3, 1259–1267.
Zeng C, He D, Brinkley BR (1994). Localization of NuMA protein isoforms in the nuclear matrix of mammalian cells. Cell Motil Cytoskeleton 29, 167–176.
Zheng Z, Wan Q, Meixiong G, Du Q (2014). Cell cycle-regulated membrane binding of NuMA contributes to efficient anaphase chromosome separation. Mol Biol Cell 25, 606–619.